


Sublattice-selective percolation on bipartite planar lattices

Jonas Wattendorff  and Stefan Wessel 

Institute for Theoretical Solid State Physics, RWTH Aachen University, JARA Fundamentals of Future Information Technology, and JARA Center for Simulation and Data Science, 52056 Aachen, Germany

 (Received 3 February 2024; accepted 11 March 2024; published 4 April 2024)

In conventional site percolation, all lattice sites are occupied with the same probability. For a bipartite lattice, sublattice-selective percolation instead involves two independent occupation probabilities, depending on the sublattice to which a given site belongs. Here, we determine the corresponding phase diagram for the two-dimensional square and Lieb lattices from quantifying the parameter regime where a percolating cluster persists for sublattice-selective percolation. For this purpose, we present an adapted Newman-Ziff algorithm. We also consider the critical exponents at the percolation transition, confirming previous Monte Carlo and renormalization-group findings that suggest sublattice-selective percolation belongs to the same universality class as conventional site percolation. To further strengthen this conclusion, we finally treat sublattice-selective percolation on the Bethe lattice (infinite Cayley tree) by an exact solution.

DOI: [10.1103/PhysRevE.109.044108](https://doi.org/10.1103/PhysRevE.109.044108)

I. INTRODUCTION

Percolation provides a remarkably simple route to non-trivial critical phenomena, which have a broad range of applications in many fields of science and engineering [1,2]. In its most basic formulation, one considers an infinite periodic lattice, occupying each lattice site independently with equal probability p . The occupied sites form contiguous clusters of connected lattice sites, which turn out to exhibit several interesting properties. In particular, an infinite, spanning (percolating) cluster of connected occupied sites emerges for sufficiently large values of p beyond a particular threshold value p_c . For example, considering a two-dimensional square lattice, the site percolation threshold $p_c^{\text{sq}} = 0.592\,746\dots$ [3,4] is known from computational studies to rather high accuracy – the exact value being, however, unknown to date. In the vicinity of the percolation threshold, various characteristics of the cluster distribution exhibit nontrivial scaling behavior: For $p \gtrsim p_c$, the strength P of the percolating cluster, i.e., the probability that a given site belongs to the percolating cluster, increases with p by an asymptotic power law,

$$P \propto (p - p_c)^\beta, \quad (1)$$

resembling the scaling behavior of an order parameter near a thermal ordering phase transition. Upon approaching p_c , the correlation length ξ , defined as the mean distance between two sites belonging to the same finite cluster, increases as

$$\xi \propto |p - p_c|^{-\nu}, \quad (2)$$

and the mean number of sites of a finite cluster S increases as

$$S \propto |p - p_c|^{-\gamma}, \quad (3)$$

corresponding to the order parameter susceptibility in thermal ordering transitions. The scaling exponents describe the critical behavior at the percolation transition of the above state functions, and they are considered universal in the sense that within a given dimension d they do not depend on details of

the lattice structure (e.g., square or triangular in $d = 2$) or the kind of percolation problem considered (site, bond, or also in the continuum) [2]. For $d = 2$ the exponents are known as $\beta = 5/36 = 0.13\bar{8}$, $\nu = 4/3$, and $\gamma = 43/18 = 2.3\bar{8}$, respectively [2,5]. Furthermore, at the percolation threshold, the infinite cluster has a fractal dimension $d_f = d - \beta/\nu$, e.g., $d_f = 91/48 = 1.895\,8\bar{3}$ for the two-dimensional case.

In physical systems the lattice sites considered above may represent objects such as atoms in a solid-state crystal, an empty site being related to a defect, e.g., an impurity atom. In many condensed-matter systems, the underlying lattice structure shows further characteristics, such as being bipartite, i.e., the total set of lattice sites can be decomposed into two disjoint sublattices, denoted A and B in the following, with nearest-neighbor sites always belonging to different sublattices (cf. Fig. 1 for two examples). If, for example in a binary system, the objects occupying the A and B sublattice are of different species, it becomes feasible that the susceptibility to a defect differs on the A and B sublattice. In the context of site percolation, such a circumstance can be described by assigning two different occupation probabilities p_A and p_B to sites from sublattices A and B , respectively. Such sublattice-selective percolation was introduced by Scholl and Binder in Ref. [6], motivated by the properties of diluted magnetic compounds, with a special focus towards experimental findings in three-dimensional spinel structures. For the latter case, they performed Monte Carlo simulations to extract the phase diagram in terms of percolating versus nonpercolating regimes of parameters (p_A, p_B) , and they provided numerical evidence that the critical exponents of sublattice-selective percolation are those of the universality class for conventional site percolation (where $p_A = p_B$). Reference [6] also considered several other lattice structures, both in three and two dimensions, focusing on the extreme case in which one sublattice is fully occupied, e.g., $p_B = 1$. In various cases, the critical value $p_{A,c}$ for p_A can then be expressed in terms of the percolation threshold of certain related conventional percolation

problems. For example, for a square lattice with $p_B = 1$, the threshold value $p_{A,c}$ equals the site percolation threshold for a square lattice with next-nearest-neighbor connectivity. Using the concept of matching lattices, this value can furthermore be shown to be equal to $1 - p_c^{\text{sq}} = 0.407253\dots$ [7]. For $p_B = 1$, the percolation threshold for p_A thus falls below the value of p_c^{sq} , as expected, since half of the lattice is already occupied for $p_B = 1$. Due to the equivalence between the two sublattices of the square lattice, the problem is symmetric under the exchange of p_A and p_B in this case. In particular, $p_{B,c} = 1 - p_c^{\text{sq}}$ along the line $p_A = 1$, and along the symmetric line $p_A = p_B$, the critical value p_c^{sq} is recovered. A quantification of the full boundary line in the (p_A, p_B) -plane of the percolating regime, however, was not performed in Ref. [6] for the basic square lattice case. Later, approximate renormalization-group (RG) calculations were used to estimate this boundary line [8] and to address the question of universality (the method was furthermore employed to study sublattice-selective percolation on other lattices and sublattice geometries [9,10]). However, while the RG approach finds that sublattice-selective percolation is indeed controlled by the same fixed point as the uniform case, its numerical accuracy is limited. For example, in the uniform case a best estimate of 0.610 was obtained for p_c^{sq} [8]. Related work, using a decoupling approximation for an effective field theory of the Ising model with sublattice-selective depletion, yields results of a similar accuracy [11,12]. Since those early works on sublattice-selective percolation, several methodological advances have been achieved, such as the Newman-Ziff algorithm [13,14], which allows for efficient high-accuracy numerical studies of conventional lattice-based percolation problems. It is thus feasible now to also perform a systematic and accurate exploration of sublattice-selective percolation on basic planar lattices, such as the square lattice using such advanced algorithms.

Here, we perform such an analysis using an adapted version of the Newman-Ziff algorithm [13,14], which we detail further below. This algorithm allows for efficient Monte Carlo studies of the phase diagram, like the original algorithm does for conventional percolation problems on periodic lattices. In addition to the square lattice, we examine the case of the planar Lieb lattice, which is also bipartite, and for which conventional site-percolation has been considered recently [15]. This lattice, which is of interest in the context of flat band physics, ferrimagnetism, and topological states, is a decorated square lattice and bipartite; cf. Fig. 1. However, in contrast to the square lattice, the two sublattices A and B of the Lieb lattice are not equivalent, and the phase diagram of sublattice-selective percolation is nonsymmetric in the (p_A, p_B) -plane. Furthermore, we use finite-size scaling in order to estimate the critical exponents for sublattice-selective percolation on the square lattice. Our results support previous conclusions [6,8] regarding the universal properties.

The remainder of this article is organized as follows: In Sec. II, we introduce an adapted Newman-Ziff algorithm for efficient computational studies of sublattice-selective percolation. Then, we report our results for the square and Lieb lattice in Secs. III and IV, respectively. Finally, in Sec. V, we study sublattice-selective percolation on the Bethe lattice, which in various aspects corresponds to infinite dimension, $d = \infty$, for

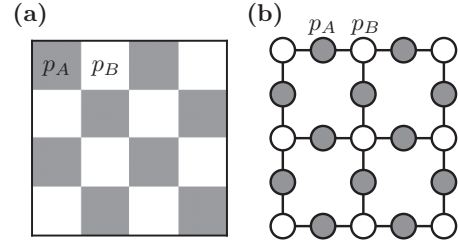


FIG. 1. Illustration of the square (a) and Lieb lattice (b). Sites from sublattices A and B are shown in gray (white). The square lattice is shown as a checkerboard, while the nearest-neighbor bonds of the Lieb lattice are shown explicitly.

coordination numbers $z \geq 3$, cf. Fig. 2 for an illustration for $z = 3$. We determine the critical exponents analytically for the cases $z = 2$ (corresponding to the chain, $d = 1$) and $z = 3$, thereby demonstrating explicitly the anticipated universality. Our final conclusions are given in Sec. VI.

II. BIPARTITE NEWMAN-ZIFF ALGORITHM

The Newman-Ziff algorithm [13,14] performs Monte Carlo sampling of the percolation problem on finite lattices of linear size L and with $N \propto L^2$ lattice sites in two dimensions. For a given system size, one measures appropriate finite-size estimators Q_L for any of the state functions Q , such as the quantities P , ξ , and S introduced above. In the following, we consider finite systems with periodic boundaries, and a cluster is defined to be percolating if it completely wraps around in either direction. The main idea behind the Newman-Ziff algorithm can be loosely described as first calculating a given state function Q_L in the microcanonical ensemble and then transforming to the canonical ensemble. In the microcanonical ensemble for a bipartite lattice, the state function is a function $Q_L(n_A, n_B)$ of the number of occupied sites n_A and n_B for each sublattice, while in the canonical ensemble it is a function of the probabilities, $Q_L(p_A, p_B)$. This is an analogy to thermodynamics, where n_A corresponds to the energy of the system and p_A corresponds to the temperature.

To explore the phase diagram, we take cuts for fixed values of p_B , which means populating each site on the B sublattice with probability p_B and then successively and randomly adding sites to the A sublattice until it is full, thus calculating $Q_L(n_A, p_B)$ for all values of n_A . Then the transformation to the canonical ensemble, i.e., $Q_L(n_A, p_B) \rightarrow Q_L(p_A, p_B)$, is

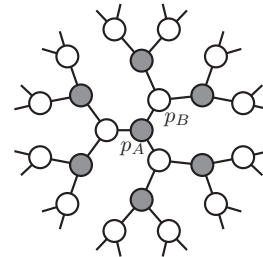


FIG. 2. Illustration of the Bethe lattice for $z = 3$. Sites from sublattices A and B are shown in gray (white). Note that for the infinite lattice, all sites are in fact topologically equivalent.

performed for the A sublattice only. For a given value of p_A , the probability $B(N_A, n_A, p_A)$ that there are exactly n_A sites occupied from the total number of N_A sites of the A sublattice is given by

$$B(N_A, n_A, p_A) = \binom{N_A}{n_A} p_A^{n_A} (1 - p_A)^{N_A - n_A}, \quad (4)$$

since choosing the occupied sites is a Bernoulli process. Weighing the (with respect to the A sublattice) microcanonical state function $Q_L(n_A, p_B)$ by the probability in Eq. (4) and summing over all values of n_A gives the canonical state function $Q_L(p_A, p_B)$,

$$Q_L(p_A, p_B) = \sum_{n_A=0}^{N_A} B(N_A, n_A, p_A) Q_L(n_A, p_B), \quad (5)$$

which is essentially a convolution with the binomial distribution. This transformation is again analogous to thermodynamics, where the transformation is performed via the Boltzmann distribution instead of the binomial distribution.

The efficiency of the Newman-Ziff algorithm derives from the fact that the number of samples for p_A is only limited by the cost of the transformation in Eq. (5) and that this transformation is linear in the state function Q_L . Hence, only the average of the microcanonical state function after many Monte Carlo steps has to be transformed explicitly,

$$\langle Q_L(p_A, p_B) \rangle = \sum_{n_A=0}^{N_A} B(N_A, n_A, p_A) \langle Q_L(n_A, p_B) \rangle. \quad (6)$$

The algorithm thus consists of three main steps. First, every site on the B sublattice is occupied with a given probability p_B , as seen in the example of Fig. 3(a). Since the lattice is bipartite, there are no clusters of size greater than single sites at this point.

Second, sites on the A sublattice are randomly occupied according to a random permutation of the sublattice indices. Every time a site is occupied, one checks each nearest neighbor one by one, and if the neighbor is occupied and belongs to a different cluster, these are merged using a union-find routine, as in the original Newman-Ziff algorithm. Every time a site is newly occupied, the state functions $Q_L(n_A, p_B)$ are added to the mean $\langle Q_L(n_A, p_B) \rangle$. In Fig. 3(b), the state in which the cluster first percolates (with periodic boundary conditions) is shown. In Fig. 3(c), the lattice is shown after adding 75 occupied sites, and only a few small clusters besides the percolating cluster remain.

Third, all the state functions are transformed according to Eq. (6). The binomial coefficients are computed recursively [14], as

$$B(N_A, n_A, p_A) = \begin{cases} B(N_A, n_A - 1, p_A) \frac{N_A - n_A + 1}{n_A} \frac{p_A}{\bar{p}_A}, \\ B(N_A, n_A + 1, p_A) \frac{n_A + 1}{N_A - n_A} \frac{\bar{p}_A}{p_A}, \end{cases}$$

for $n_A > p_A N_A$ and $n_A < p_A N_A$, respectively, with $\bar{p}_A = 1 - p_A$. In practice, $B(N_A, n_A, p_A)$ is negligible for many values of n_A , so only seven standard deviations $\sqrt{p_A(1 - p_A)N_A}$ around the maximum value $p_A N_A$ are actually calculated, which only excludes $B(N_A, n_A, p_A) \lesssim 10^{-10}$.

In the actual implementation, the lattice is represented by an integer array of size N . If a site is occupied, it is part of

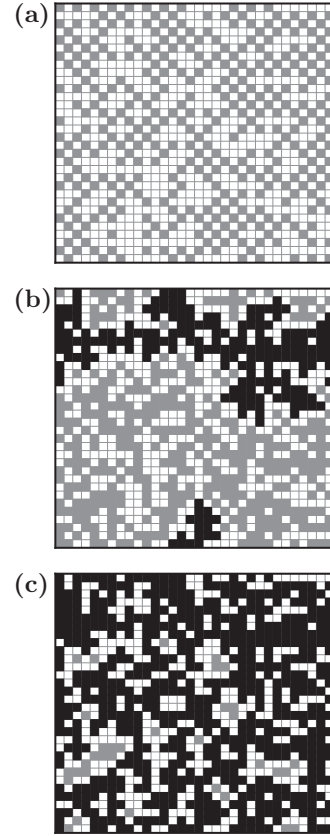


FIG. 3. Illustration of the sublattice-selective percolation process for an $L = 32$ square lattice and periodic boundary conditions. Occupied (empty) sites are shown in gray (white), and the percolating cluster is in black. Starting from a random occupation of the B sublattice sites with probability $p_B = 0.7$, the A sublattice is empty in (a), filled by $n_A = 225$ sites in (b), and $n_A = 300$ sites in (c).

a tree, and each tree corresponds to one cluster. A cluster of size s has one root, which has an array entry of value $-s$, while the other sites of the cluster have pointers (indices of the array) which eventually lead to the root. The idea behind the aforementioned union-find algorithm is that the union operation merges two trees and the find operation returns the root of a given occupied site. So if there are two neighboring occupied sites on the lattice, the roots can be compared via find, and if the roots are different, the trees will be merged via union. Figure 4 shows an example of this procedure. The light gray site in Fig. 4(a) has been newly added, making it a tree just consisting of a root. Next, it is merged with the right cluster in Fig. 4(b), making a larger cluster of size $s = 5$. In the next step in Fig. 4(c), the roots of the light gray site and the site to the left of it are compared via the find operation, and the roots are at different lattice sites. Thus, the union operation is invoked, and the root of the left tree then points to the root of the right tree and the cluster sizes are added. Now every site in the cluster returns the same root with find. There are a couple of methods to make this procedure more efficient: First, the so-called path compression is the idea that the find operation is most efficient when the path to the root involves as few pointers as possible. So every time the find operation follows a path from some site to the root, all the pointers on its way

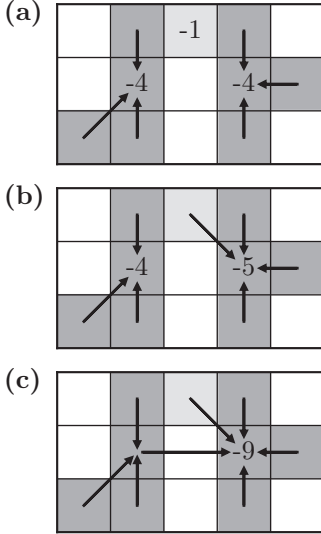


FIG. 4. Example of adding a newly occupied site on a square lattice. Gray sites are occupied, and the light gray site is newly occupied. The roots are marked by negative numbers, and the arrows symbolize pointers.

are set to point directly to the root—in practice, this makes the trees never deeper than a few generations. Second, a smaller cluster is always appended to a bigger one. The find operation for the cluster that is appended takes one step longer, hence by appending the smaller cluster, the average number of steps is again minimized.

In terms of computational complexity, using approaches based on alternative methods, such as the Hoshen-Kopelman algorithm [16], one would have to build all clusters for every value of p_A from scratch, and the time complexity would be $O(N_A^2)$ for each realization for a given value of p_B . In contrast, the Newman-Ziff algorithm takes time of order $O(N_A + M_T)$ to calculate the N_A samples of $Q_L(n_A, p_B)$ and transform from the microcanonical to the canonical ensemble, where M_T is the number of steps needed to calculate the sum and binomial distribution in the transformation of Eq. (6). For the system sizes used here, M_T and thus the computational time for the transformation are comparably small. For a detailed discussion of the computational advantage of the Newman-Ziff algorithm, we refer the reader to Ref. [14].

III. SQUARE LATTICE

We used the bipartite Newman-Ziff algorithm algorithm to examine sublattice-selective percolation on the square lattice, and we report our numerical results in this section.

A. Percolation threshold

We first consider the determination of the percolation threshold line for sublattice-selective percolation on the square lattice. As noted in the previous section, for this purpose we consider a set of fixed values of p_B , and then we use the bipartite Newman-Ziff algorithm to obtain $Q_L(p_A, p_B)$ for essentially any value of p_A . Denoting by R_L the probability for the existence of a percolating cluster (and estimated

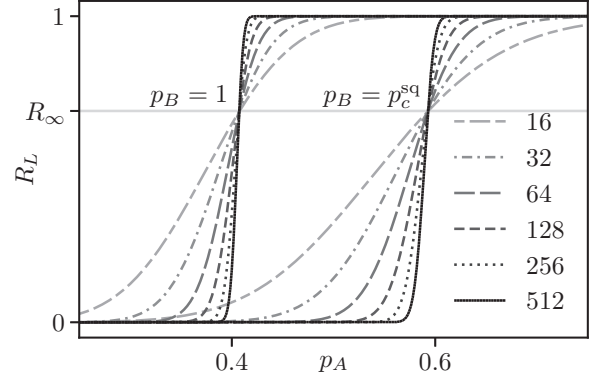


FIG. 5. Numerical results for the dependence of R_L as a function of p_A for different values of L for sublattice-selective percolation on the square lattice for $p_B = 1$ (left curves) and $p_B = p_c^{\text{sq}}$ (right curves). The horizontal line indicates the exact value of R_∞ at p_c^{sq} from Ref. [14].

by the Monte Carlo mean), this state function increases monotonously from 0 to 1 smoothly upon increasing p_A for finite L . This behavior is shown for two different values of p_B in Fig. 5, considering $p_B = p_c^{\text{sq}}$ and $p_B = 1$, respectively.

In the infinite system limit, this quantity—denoted $R_\infty(p_A)$ —exhibits a jump at the percolation threshold, and we can obtain an estimate $p_{A,c}(L)$ of $p_{A,c}$ at the specified value of p_B from the condition $R_L(p_{A,c}(L)) = C$, where $C \in (0, 1)$ is kept fixed upon varying L . The speed of convergence of $p_{A,c}(L)$ towards $p_{A,c}$ varies for different choices of C . For conventional site percolation, Newman and Ziff [14] suggest taking C equal to the exactly known value of R_∞ at p_c^{sq} , which equals $0.6904\dots$, and finding an algebraic asymptotic convergence,

$$p_{A,c}(L) - p_{A,c} \propto L^{-X}, \tag{7}$$

conjecturing that $X = 2 + 1/\nu$, which equals 2.75 for $d = 2$, leading thus to fast convergence. From our simulations, we observe no significant change in the threshold value of R_∞ for the sublattice-selective case (cf., e.g., the crossing point values in Fig. 5). A formal proof of this statement would, however, still be valuable. In any case, we always fixed C to the above value in order to fit $p_{A,c}(L)$ to the finite-size scaling in Eq. (7).

In particular, we performed finite-size calculations for system sizes between $L = 16$ and 512, doubling consecutive values of L . For each fixed value of p_B , we scaled the number of Monte Carlo steps [each corresponding to an initial configuration as in Fig. 3(a), followed by successively increasing n_A] with $L^{-3/2}$, taking 10^7 steps at $L = 16$. This procedure ensures a similar absolute statistical uncertainty on the estimator for $R_L(p_{A,c}(L))$ upon varying L , as it does for conventional percolation [14]: For a given probability p_A , the state function $R_L(p_A)$ is either 1 or 0, so the uncertainty comes from the binomial distribution,

$$\sigma_{R_L} = \sqrt{\frac{R_L(p_A)[1 - R_L(p_A)]}{M}}, \tag{8}$$

where M is the number of Monte Carlo steps. As the width of the critical region decreases as $L^{-1/\nu}$, the gradient dR_L/dp_A of $R_L(p_A)$ in the critical region increases as $L^{1/\nu}$. Together

TABLE I. Numerical results obtained for sublattice-selective percolation on the square lattice using the bipartite Newman-Ziff algorithm.

p_B	$p_{A,c}$	X	ν
p_c^{sq}	0.5927483(16)	2.80(10)	1.3318(4)
0.65	0.5431265(18)	2.66(13)	1.331(4)
0.7	0.5095937(13)	2.49(7)	1.3290(7)
0.75	0.4826738(13)	2.42(7)	1.3340(6)
0.8	0.46082758(35)	2.561(18)	1.3352(10)
0.85	0.4430110(13)	2.60(6)	1.3368(12)
0.9	0.4284801(17)	2.56(8)	1.3324(28)
0.95	0.4166941(8)	2.598(34)	1.3321(4)
1	0.4072524(6)	2.556(21)	1.3337(5)

with Eq. (8), the uncertainty on $p_{A,c}$ thus scales as $\sigma_{p_{A,c}} \sim L^{-1/\nu} \sigma_{R_L} \sim L^{-1/\nu} M^{-1/2}$. To keep $\sigma_{p_{A,c}}$ constant, M thus has to scale with $L^{-2/\nu}$. For $d = 2$, the universal value is $\nu = 4/3$, and this value will also be used for this uncertainty calculation here (this has no impact on the estimation of the critical exponents as performed in the next section—there will indeed also be no evidence that $\nu \neq 4/3$). Overall, the whole procedure was repeated 100 times for a given p_B in order to obtain the statistical error on all other estimated state functions. For the final transformation from n_A to p_A , we used a narrow p_A grid with a spacing of order 10^{-4} .

Based on the numerical data, we obtain the values of $p_{A,c}$ for several values of p_B reported in Table I. Also included in this table are the values of the exponent X that we obtain based on these fits [the values of $\chi^2/\text{d.o.f.}$ (degree of freedom) are of $O(1)$]. Overall, the estimated values of X exhibit some scatter, but no significant systematic deviation from the proposed value for the conventional case [14]. The numerical results for $p_{A,c}$ that we obtain for the specific cases of $p_B = p_c^{\text{sq}}$ and $p_B = 1$ are in accord with the previously reported values, ensuring the overall accuracy of our approach. Based on the numerical values of $p_{A,c}$, and using the symmetry under the exchange of p_A and p_B , we obtain the phase diagram for sublattice-selective percolation on the square lattice shown in Fig. 6.

B. Critical exponents

In addition to the percolation threshold, we estimated the critical exponents for sublattice-selective percolation on the square lattice using appropriate finite-size scaling analysis [2]. We first consider the critical exponent ν , which can best be estimated from the finite-size scaling of the gradient $R'_L = dR_L/dp_A$ of $R_L(p_A)$ near the percolation threshold,

$$R'_L \propto L^{1/\nu}. \quad (9)$$

We approximate R'_L from the slope of a linear regression within a p_A range of 10^{-3} around the estimated value of $p_{A,c}$. The thus obtained estimates for ν are given in Table I, and Fig. 7 shows best fits to the numerical data for different values of p_B . The values that we obtain for ν scatter with no systematic dependence of p_B , and taking their average gives $\nu = 1.3352(11)$, which is in good agreement with $\nu = 4/3$ for the $d = 2$ universality class. We also find no indication that

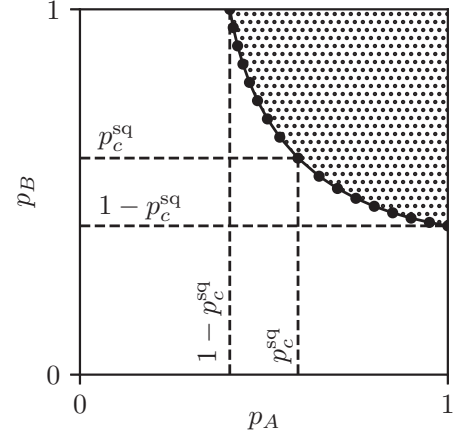


FIG. 6. Phase diagram for sublattice-selective percolation on the square lattice, as obtained from the bipartite Newman-Ziff algorithm. The dotted regime is percolating.

the critical exponents β and γ differ from their conventional values for $d = 2$. To access these exponents, we consider the finite-size scaling forms

$$P_L = L^{-\beta/\nu} F_P[L^{1/\nu}(p_A - p_{A,c})] \quad (10)$$

for the estimate P_L of the strength of the percolating cluster in terms of a scaling function F_P , and similarly

$$S_L = L^{\gamma/\nu} F_S[L^{1/\nu}(p_A - p_{A,c})] \quad (11)$$

for the mean number S of finite clusters. From appropriate data-collapse plots, one can adjust the values of β and γ , based on our previous estimates for ν and $p_{A,c}$, in order to obtain the best collapse within the critical region. Using such an analysis, we find that the best-fit values are in fact in accord with the known values for conventional percolation in $d = 2$. This is illustrated for several values of p_B in Fig. 8. We thus conclude from our finite-size analysis that the critical exponents for sublattice-selective percolation are in agreement with the universal values for $d = 2$ percolation, supporting previous findings [6,8].

IV. LIEB LATTICE

As a further example, we examine sublattice-selective percolation on the Lieb lattice, for which the case of uniform site percolation ($p_A = p_B$) has recently been considered [15].

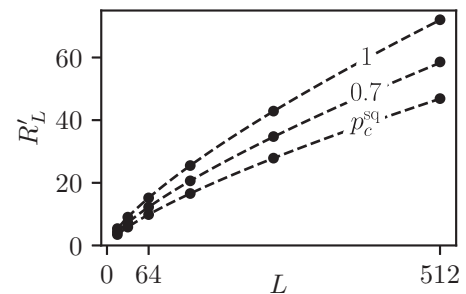


FIG. 7. Fits of the numerical data for R'_L to the finite-size scaling form in Eq. (9) for different indicated values of p_B .

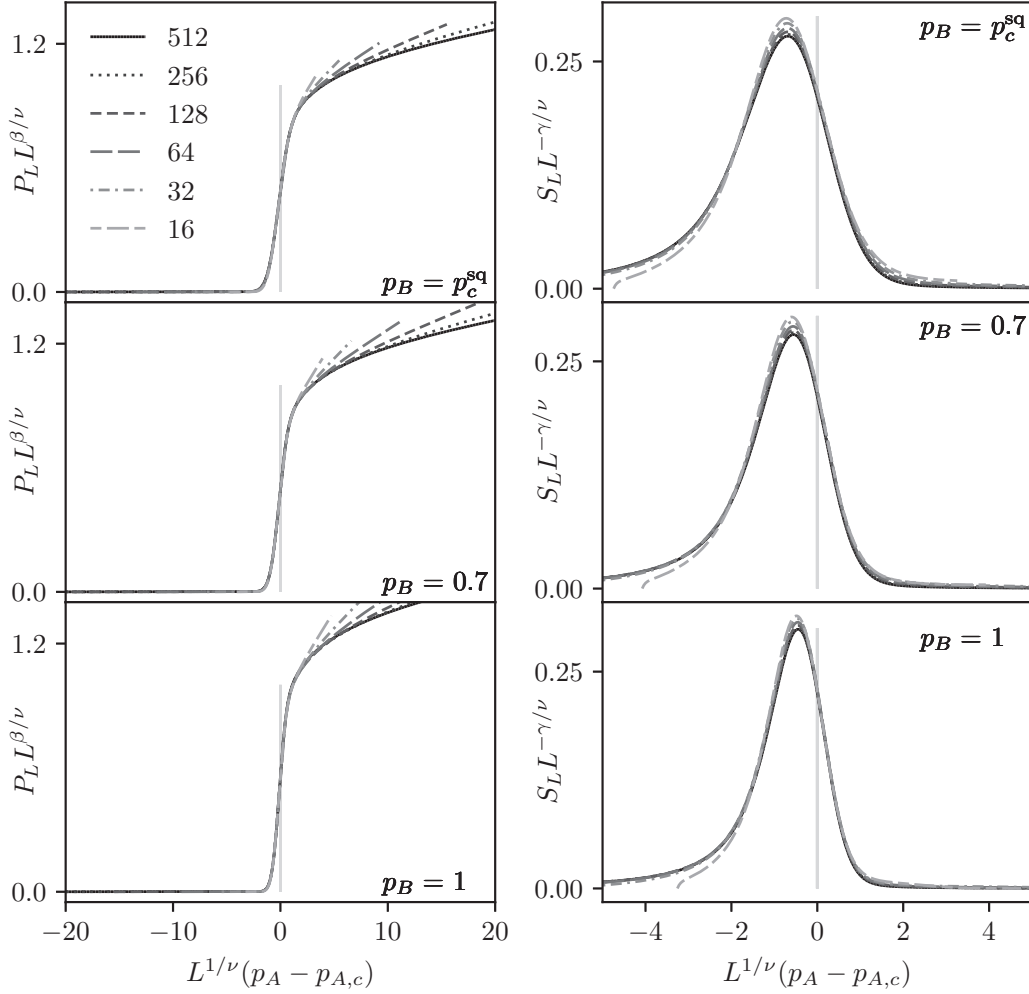


FIG. 8. Data collapse plots for finite-size data labeled by L for P and S for different values of p_B using the critical exponents for $d = 2$ percolation.

Since the Lieb lattice is in fact a decorated square lattice, sublattice-selective percolation is equivalent in this case to mixed bond-site percolation on the square lattice, with p_A (p_B) specifying the bond (site) occupation probability. In particular, in the limit $p_A = 1$ ($p_B = 1$), we obtain conventional pure site (bond) percolation on the square lattice, and thus $p_{B,c} = p_c^{\text{sq}}$ ($p_{A,c} = 1/2$) along these lines, respectively (here, we used the fact that the percolation threshold $1/2$ for bond percolation on the square lattice has been exactly determined [17]). This shows explicitly that due to the inequivalence of the two sublattices of the Lieb lattice, the phase diagram is not symmetric in the (p_A, p_B) -plane. In Ref. [18], the general case of mixed bond-site percolation is considered for various lattices, including the square lattice (mixed bond-site percolation on several lattices is also considered in Refs. [19–22]). The phase diagram was numerically estimated, but only to comparably low accuracy, so that here we employed the bipartite Newman-Ziff algorithm in order to obtain more accurate values for the threshold line for sublattice-selective percolation on the Lieb lattice. The numerical results are provided in Table II, and the corresponding phase diagram is shown in Fig. 9. Comparing the value of $p_{A,c}$ obtained for $p_B = 1$ to the exact value ($1/2$) confirms the accuracy

of our results. For estimating these numbers, C was chosen identical to the square lattice value from the previous section, resulting in similarly fast convergence. Additionally, the previous estimate [15] for the conventional ($p_A = p_B$) site percolation threshold p_c^{Lieb} on the Lieb lattice was improved using the Newman-Ziff algorithm. Along this line, we find

TABLE II. Numerical results obtained for sublattice-selective percolation on the Lieb lattice using the bipartite Newman-Ziff algorithm.

p_B	$p_{A,c}$
0.6	0.983336(4)
0.65	0.8809405(10)
0.7	0.7965947(21)
0.75	0.7261839(20)
0.8	0.6666702(16)
0.85	0.6157944(18)
0.9	0.5718775(14)
0.95	0.5336113(21)
1	0.4999987(19)

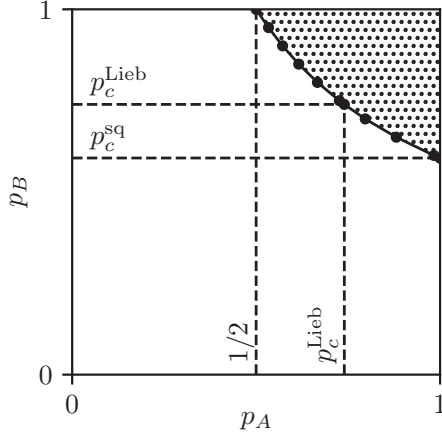


FIG. 9. Phase diagram for sublattice-selective percolation on the Lieb lattice, as obtained from the bipartite Newman-Ziff algorithm. The dotted regime is percolating.

that $C = 0.68$ yields better convergence (however, even then the exponent $X \approx 1/\nu$ is significantly lower). The obtained value $p_c^{\text{Lieb}} = 0.7397120(17)$ is consistent with the previous best estimate [15].

V. BETHE LATTICE

To complement the above numerical study by exact analytical results, we finally consider sublattice-selective percolation on the Bethe lattice. We first consider the case $z = 2$, essentially corresponding to the one-dimensional chain.

A. Percolation on a chain ($z = 2$)

In this case, percolation occurs only at the singular point $(p_A, p_B) = (1, 1)$. To extract the critical exponents upon approaching the percolation point along different lines within the (p_A, p_B) -plane, we next examine appropriate state functions.

A cluster containing s occupied sites with one empty site to either side is called an s -cluster. The number of s -clusters per lattice site n_s is a useful state function. Another way of looking at n_s is that it is the probability of an arbitrary site to be the left-end site of an s -cluster. This is the case if the site to the left is empty, then s consecutive sites are occupied, followed by another empty site. For $p_A = p_B = p$, the state function would be $n_s = (1-p)p^2(1-p)$, but for $p_A \neq p_B$ one has to consider whether the left end site is from the A or B sublattice, and whether s is even or odd. The probability that an arbitrary site is from the A or B sublattice is equal to $1/2$, and from thereon it is a matter of counting the A - and B -sublattice sites in the cluster to find

$$n_s(p_A, p_B) = \frac{1}{2}((\bar{p}_B)^2 p_A + (\bar{p}_A)^2 p_B) p_A^{(s-1)/2} p_B^{(s-1)/2} \quad (12)$$

for odd s , and

$$n_s(p_A, p_B) = \bar{p}_A \bar{p}_B p_A^{s/2} p_B^{s/2} \quad (13)$$

for even s , where $\bar{p}_A = 1 - p_A$, $\bar{p}_B = 1 - p_B$. The probability that an arbitrary site is part of an s -cluster is $n_s(p_A, p_B)s$, so the probability that an arbitrary site is part of any cluster is

given by

$$\sum_{s=1}^{\infty} n_s(p_A, p_B)s = \frac{1}{2}(p_A + p_B), \quad (14)$$

i.e., equivalent to the probability that an arbitrary site is occupied. From n_s , the mean cluster size S can be evaluated, which equals the ratio of the second divided by the first moment of the cluster size distribution,

$$\begin{aligned} S(p_A, p_B) &= \frac{\sum_{s=1}^{\infty} n_s(p_A, p_B)s^2}{\sum_{s=1}^{\infty} n_s(p_A, p_B)s} \\ &= \frac{p_A^2 p_B + p_A p_B^2 + 4p_A p_B + p_A + p_B}{p_A + p_B - p_A^2 p_B - p_A p_B^2}, \end{aligned} \quad (15)$$

which approaches 1 for $(p_A, p_B) \rightarrow (0, 0)$ and diverges upon approaching $(1, 1)$. We obtain the critical exponent γ from analyzing the singular behavior of S near $(1, 1)$. Fixing $p_B = 1$, the asymptotic singularity is obtained as

$$\begin{aligned} S(p_A, 1) &= \frac{p_A^2 + 6p_A + 1}{1 - p_A^2} \\ &\sim 4(1 - p_A)^{-1} \quad \text{for } p_A \sim 1, \end{aligned} \quad (16)$$

so that $\gamma = 1$. This asymptotic scaling also results upon approaching $(1, 1)$ along any other line. Namely, for $p_A = 1 - r \cos(\phi)$, $p_B = 1 - r \sin(\phi)$, with $\phi \in [0, \pi/2]$, the asymptotic behavior $S \sim 4/[\cos(\phi) + \sin(\phi)]r$ for $r \rightarrow 0$ is obtained.

To obtain the correlation length ξ , we first calculate the correlation function (pair connectivity function) $g(r)$, which equals the mean number of sites that are in the same cluster as a given occupied site, at a distance r apart. Thus, there have to be $r - 1$ consecutive occupied sites in between. For $p_A = p_B = p$ this is just $2p^r$ (2 for both directions), but for $p_A \neq p_B$ the parity of r and the starting site have to be accounted for. The starting site is on the A sublattice with probability $\frac{p_A}{p_A + p_B}$ and on the B sublattice with probability $\frac{p_B}{p_A + p_B}$. Accounting for the parity of r and the special case $r = 0$, we obtain

$$g(r) = \begin{cases} 1, & r = 0, \\ \frac{4}{p_A + p_B} p_A^{(r+1)/2} p_B^{(r+1)/2}, & r \text{ odd}, \\ 2p_A^{r/2} p_B^{r/2}, & r \text{ even}. \end{cases} \quad (17)$$

The correlation length ξ quantifies the lengthscale of the correlation function, and can also be viewed as the radius of the clusters that give the main contribution to the mean cluster size S [2]. The formal definition is

$$\xi^2 = \frac{\sum_r r^2 g(r)}{\sum_r g(r)}. \quad (18)$$

A well-known identity in conventional percolation is that the sum over all $g(r)$ equals the mean cluster size, and this indeed also follows for sublattice-selective percolation, as we obtain

$$\sum_{r=0}^{\infty} g(r) = S. \quad (19)$$

The numerator in Eq. (18) can also be calculated, and for $p_B = 1$ it scales as $(1 - p_A)^{-3}$ near the percolation threshold.

Since $1/S$ scales as $(1 - p_A)$, the singularity of ξ is thus obtained as

$$\xi^2(p_A, 1) = \frac{\sum_r r^2 g(r)}{S} \sim (1 - p_A)^{-2} \quad \text{for } p_A \sim 1, \quad (20)$$

and we extract the critical exponent $\nu = 1$ for the divergence of ξ near the percolation threshold.

The third state function that we consider is the strength of the percolating cluster P . For the chain this function is trivially 1 for $p_A = p_B = 1$ and 0 otherwise. P is thus constant with a discontinuity at the percolation threshold, and $\beta = 0$.

In summary, for the one-dimensional case, the critical exponents for sublattice-selective percolation, specifying the behavior at the singular point $p_A = p_B = 1$, are given by $\beta = 0$, $\nu = 1$, $\gamma = 1$. These are the same exponents as for conventional percolation in $d = 1$ [2]. Since only $p_A = p_B = 1$ percolates, this conclusion may not be surprising.

B. Percolation threshold line for general z

The percolation condition on the Bethe lattice is that a chain of occupied sites reaches out to infinity. In other words, the system percolates if from some occupied site there exists a path of connected occupied sites that never ends (note that on the Bethe lattice such a path cannot form loops). If a chain of sites from a specific site up to some other site are occupied, at least one of the two neighbors going outwards also has to be occupied to have a percolating cluster. Hence, the mean number of occupied sites going outwards has to be at least 1 in order to form a percolating cluster. Furthermore, on the Bethe lattice the A and B sublattices alternate. The mean number of occupied sites going outwards can thus be calculated for z neighbors by using two nested binomial distributions, one accounting for the mean number of A -sublattice sites and the other for the mean number of B -sublattice sites. This leads to the condition

$$1 \stackrel{!}{=} \sum_{k=0}^{z-1} \binom{z-1}{k} p_A^k (1 - p_A)^{z-1-k} \times \sum_{l=0}^{(z-1)k} \binom{(z-1)k}{l} p_B^l (1 - p_B)^{(z-1)k-l}, \quad (21)$$

which can be simplified to yield the condition for the percolation transition,

$$p_A p_B = \frac{1}{(z-1)^2}. \quad (22)$$

Note that this result is also correct for $z = 2$, treated in the previous section. The percolation threshold line for $z = 3$ is at $p_A p_B = 1/4$, which is plotted in Fig. 10. The larger z is, the bigger the area of the phase diagram that is percolating, but here only $z = 3$ will be further examined.

C. Scaling exponents for $z = 3$

To access the critical exponents, three state functions will again be calculated: The strength of the percolating cluster P , the mean cluster size S , and the correlation length ξ . Here, we focus on $z = 3$.

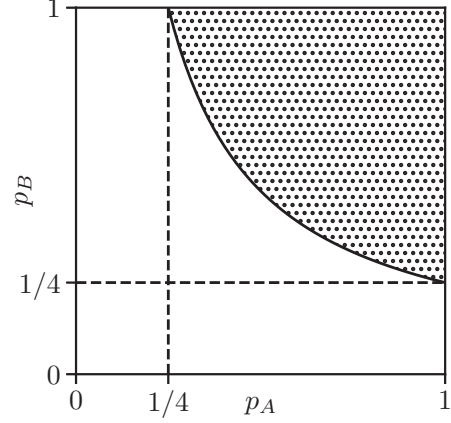


FIG. 10. Phase diagram of sublattice-selective percolation on the Bethe lattice for $z = 3$.

To obtain P , we first calculate the probability of a path leading to infinity. Let w_A (w_B) be the probability that an arbitrary A (B) sublattice site does not lead to infinity, respectively. An A sublattice site does not lead to infinity if the site itself is not occupied (given by the probability $1 - p_A$) or if the two neighbors leading outwards do not lead to infinity (given by the probability $p_A w_B^2$), and similarly for a B sublattice site. Altogether, this gives the recursive expressions

$$w_A = (1 - p_A) + p_A w_B^2, \quad (23)$$

$$w_B = (1 - p_B) + p_B w_A^2. \quad (24)$$

This nonlinear system of equations has polynomials of degree 4 as solutions. The trivial solution is $w_A = w_B = 1$, while the other real solution, denoted by w_A^P , w_B^P , is rather lengthy, and given explicitly as a function of p_A and p_B in Appendix A. We note that for larger coordination number z , the corresponding recursion equations lead to higher-order equations for w_A and w_B , for which closed expressions for the roots are known not to exist from Galois theory. For $p_A p_B < 1/4$ there exists no infinite cluster, and thus the trivial solution applies, while for $p_A p_B \geq 1/4$ the other real solution is valid, i.e.,

$$w_{A/B} = \begin{cases} 1, & 4p_A p_B < 1, \\ w_{A/B}^P(p_A, p_B), & 4p_A p_B \geq 1. \end{cases} \quad (25)$$

From these probabilities, the strength of the percolating cluster P can be calculated as

$$P(p_A, p_B) = \frac{1}{2}(p_A(1 - w_B^3) + p_B(1 - w_A^3)), \quad (26)$$

since the probability that the center site is from the A or B sublattice is $1/2$ and the probability that the site is occupied and at least one neighbor leads to infinity equals $p_{A/B}(1 - w_{B/A}^3)$. The strength of the percolating cluster is plotted in Fig. 11. In Fig. 12, cuts of P at three different values of p_B are shown, along with the function $6p_A p_B - 3/2$, which yields the leading asymptotic of P for conventional site-percolation on the Bethe lattice [2]. We thus find that near the percolation threshold line, i.e., for $p_A \gtrsim 1/(4p_B)$, $p_B \geq 1/4$, the scaling

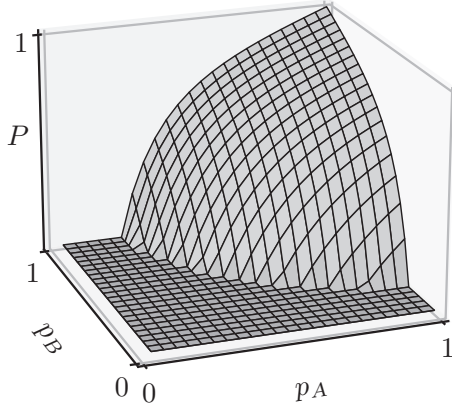


FIG. 11. Strength P of the percolating cluster for sublattice-selective percolation on the Bethe lattice for $z = 3$.

behavior

$$P(p_A, p_B) \sim -3/2 + 6p_A p_B = -6p_B \left(\frac{1}{4p_B} - p_A \right) \quad (27)$$

emerges, implying a critical exponent $\beta = 1$.

Next, the mean cluster size S will be calculated. For this, an arbitrary occupied starting site is considered and the mean mass of the cluster it belongs to is calculated. This approach is only valid below the percolation threshold line, i.e., for $4p_A p_B < 1$, because otherwise the mass of the percolating cluster has to be accounted for as well. If the starting site belongs to the A (B) sublattice, then let S_B (S_A) be the contribution to the mean cluster size from each neighbor. The mean cluster size is then composed of the contribution from the center site plus the contribution from the three neighbors, so that

$$S(p_A, p_B) = 1 + 3 \frac{1}{p_A + p_B} (p_A S_B + p_B S_A). \quad (28)$$

The contributions S_A and S_B can be accessed recursively: If the starting site belongs to the A sublattice, then a given neighbor only contributes a nonzero S_B with probability p_B . The size of this contribution is the site itself plus S_A for the two neighbors going outwards. With a similar reasoning for the B sublattice,

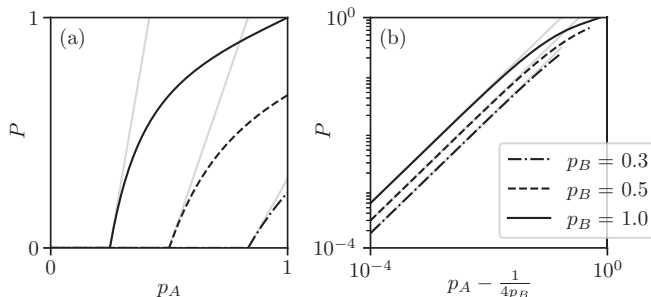


FIG. 12. Strength P of the percolating cluster as a function of p_A for various values of p_B (a) along with the function $6p_A p_B - 3/2$, and (b) in shifted log-log form near the percolation threshold.

we thus obtain

$$\left. \begin{aligned} S_A &= p_A(1 + 2S_B) \\ S_B &= p_B(1 + 2S_A) \end{aligned} \right\} \Rightarrow \begin{aligned} S_A &= \frac{2p_A p_B + p_B}{1 - 4p_B p_A}, \\ S_B &= \frac{2p_A p_B + p_A}{1 - 4p_B p_A}. \end{aligned} \quad (29)$$

Both S_A and S_B diverge upon approaching the threshold condition $p_A p_B = \frac{1}{4}$. Hence, the behavior of S near the percolation threshold line can be described by

$$S(p_A, p_B) \sim \left(\frac{1}{4p_B} - p_A \right)^{-1}, \quad (30)$$

giving the critical exponent $\gamma = 1$.

Finally, the correlation length will be calculated. Here, the topological distance r_t and the Euclidean distance r have to be distinguished. The topological distance between two sites, also called the chemical distance, is defined as the number of bonds that connect them, in contrast to the Euclidean distance, which is the distance that these points are apart in space. For $d = \infty$, the conversion becomes easy because all bonds are pairwise perpendicular, so that the Euclidean distance can be calculated by the generalized Pythagorean theorem as $r = \sqrt{r_t}$ [23].

The correlation function $g(r) = g(\sqrt{r_t})$, for $4p_A p_B < 1$, equals the mean number of occupied sites that are within the same cluster as a given occupied site, a topological distance r_t apart—corresponding to the Euclidean distance $r = \sqrt{r_t}$. At $r_t = 0$, the center site is already occupied, while at $r_t = 1$ the site has three neighbors, and from thereon the number of neighbors doubles in each step, and the probabilities are otherwise the same as for the case of the chain, so that we obtain

$$g(\sqrt{r_t}) = \begin{cases} 1, & r_t = 0, \\ 3 \times 2^{r_t-1} \frac{2}{p_A + p_B} p_A^{\frac{(r_t+1)}{2}} p_B^{\frac{(r_t+1)}{2}}, & r_t \text{ odd}, \\ 3 \times 2^{r_t-1} p_A^{\frac{r_t}{2}} p_B^{\frac{r_t}{2}}, & r_t \text{ even}. \end{cases}$$

The Euclidean correlation length can also be expressed in terms of the topological distance, since

$$\xi^2 = \frac{\sum_{r \in \{0,1,\sqrt{2},\sqrt{3},\dots\}} r^2 g(r)}{\sum_{r \in \{0,1,\sqrt{2},\sqrt{3},\dots\}} g(r)} = \frac{\sum_{r_t \in \mathbb{N}_0} r_t g(\sqrt{r_t})}{\sum_{r_t \in \mathbb{N}_0} g(\sqrt{r_t})}. \quad (31)$$

We note that the identity $\sum_r g(r) = S$ is again satisfied, and hence the denominator of Eq. (31) behaves like $(1 - 4p_A p_B)^{-1}$ for $p_A \sim 1/p_B$. Furthermore, we find that the numerator behaves like $(1 - 4p_A p_B)^{-2}$ for $p_A \sim 1/p_B$, and together the singularity of ξ near the percolation threshold is given by

$$\xi(p_A, p_B) \sim \left(\frac{1}{4p_B} - p_A \right)^{-\frac{1}{2}}, \quad (32)$$

so that $\nu = 1/2$. We thus obtain the same critical exponents as for conventional percolation on the Bethe lattice.

VI. CONCLUSIONS

We presented an adapted Newman-Ziff algorithm to examine sublattice-selective percolation on bipartite lattices, and we applied it to accurately determine the percolation threshold lines for the square lattice and the planar Lieb lattice. The latter case relates to mixed bond-site percolation on the square

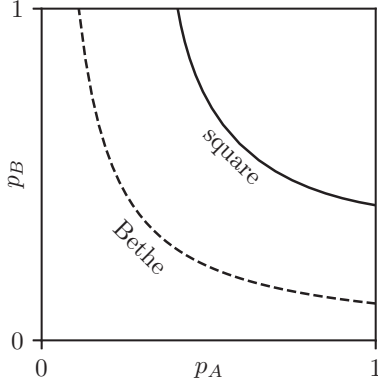


FIG. 13. Comparison between the percolation threshold line for sublattice-selective percolation on the square lattice (solid line) and the Bethe lattice with $z = 4$ (dashed line).

lattice, and our numerical results for the percolation threshold line refine previous estimates. Our numerical estimates for the critical exponents at the percolation transition are consistent with the universality class for percolation in $d = 2$.

In addition, we examined sublattice-selective percolation on the Bethe lattice, which was in fact the geometry considered in the pioneering work on percolation by Flory in the context of polymerization [1]. For this case, we obtained the exact percolation threshold line and critical exponents for $z = 2$ and 3 , which are again in accord with the values for conventional percolation. Given that the sites of the square lattice have a uniform coordination number of $z = 4$, it may be interesting to compare its phase diagram to that of the Bethe lattice with $z = 4$. Such a comparison is shown in Fig. 13, illustrating the substantially larger percolating regime for the latter case. Indeed, the absence of closed loops for a chain of connected sites leads to an overall prior appearance of the percolating cluster upon increasing the site occupation probabilities on the Bethe lattice. We checked explicitly that a rescaling of the analytic expression for the percolation threshold line for the $z = 4$ Bethe lattice to match the ends points at $p_A = 1$ and $p_B = 1$ does not fit the full numerical data.

Related to the last point, we note that the authors of Ref. [18] considered various proposed analytic expressions for the general functional form of the percolation threshold line for mixed bond-site percolation. They observed clear systematic deviations from the numerical data for low-coordinated lattices. Based on our refined data on the Lieb lattice, we can also exclude the validity of these expressions for the square lattice (cf. Appendix B). It thus remains an interesting open question for further research to derive analytical

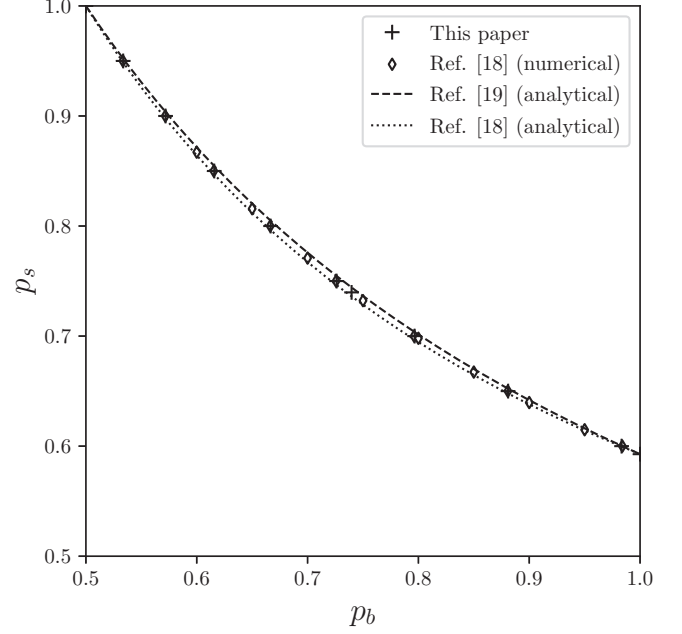


FIG. 14. Comparison between the estimates for the percolation threshold line for mixed bond-site percolation on the square lattice as obtained from the adapted Newman-Ziff algorithm, the numerical estimates from Ref. [18], as well as the analytical formulas proposed in Ref. [19] [their Eq. (3)] and Ref. [18] [their Eq. (19)], respectively.

expressions for the percolation threshold line for sublattice-selective as well as mixed bond-site percolation, respectively. We hope that our refined numerical data will be valuable as a benchmark for such investigations. Finally, let us note that sublattice-selective percolation can also be related to the problem of antisite defect percolation, such as that considered in Ref. [24] for the case of a simple cubic lattice. Certainly, the adapted Newman-Ziff algorithm can be of use also for further investigations of such generalized percolation problems.

ACKNOWLEDGMENTS

We thank Nils Caci for discussions. Furthermore, we acknowledge support by the Deutsche Forschungsgemeinschaft (DFG) through RTG 1995, and we thank the IT Center at RWTH Aachen University for access to computing time.

APPENDIX A: NONTRIVIAL REAL SOLUTION FOR THE $z = 3$ BETHE LATTICE

The nontrivial real solution to Eqs. (23) and (24), obtained using the Sympy Python library, is

$$w_{A/B}^P = -\frac{1}{3} \left(\frac{1 - a_{A/B}}{c_{A/B}} + c_{A/B} + 1 \right), \quad \text{where}$$

$$a_{A/B} = \frac{3(2 - p_{B/A})}{p_{B/A}},$$

$$b_{A/B} = \frac{27(-p_{A/B}p_{B/A}^2 + 2p_{A/B}p_{B/A} - 1)}{p_{A/B}p_{B/A}^2},$$

$$c_{A/B} = \sqrt[3]{\frac{\sqrt{-4(1 - a_{A/B})^3 + (2 - 3a_{A/B} + b_{A/B})^2}}{2} + 1 - \frac{3}{2}a_{A/B} + b_{A/B}}.$$

APPENDIX B: COMPARISON FOR MIXED BOND-SITE PERCOLATION ON THE SQUARE LATTICE

In Fig. 14, we compare our results for the transition line for mixed bond-site percolation on the square lattice (as discussed in Sec. IV, this relates to sublattice-selective percolation on the Lieb lattice) to previous numerical

estimates from Ref. [18], and two proposed analytical formulas for this transition line, taken from Ref. [19] [their Eq. (3)] and Ref. [18] [their Eq. (19)], respectively. We find that our data, based on the adapted Newman-Ziff algorithm, are in accord with the numerical estimates reported in Ref. [18] and exclude the validity of both proposed analytical formulas.

[1] P. J. Flory, *J. Am. Chem. Soc.* **63**, 3083 (1941).
 [2] D. Stauffer and A. Aharony, *Introduction to Percolation Theory* (Taylor & Francis, London, 2018).
 [3] M. J. Lee, *Phys. Rev. E* **78**, 031131 (2008).
 [4] J. L. Jacobsen, *J. Phys. A* **48**, 454003 (2015).
 [5] S. Smirnov and W. Werner, *Math. Res. Lett.* **8**, 729 (2001).
 [6] F. Scholl and K. Binder, *Z. Phys. B* **39**, 239 (1980).
 [7] M. F. Sykes and J. W. Essam, *J. Math. Phys.* **5**, 1117 (1964).
 [8] T. Idogaki and N. Uryû, *Phys. Lett. A* **90**, 367 (1982).
 [9] T. Idogaki and N. Uryu, *J. Phys. C* **15**, L1077 (1982).
 [10] T. Idogaki and N. Uryû, *J. Magn. Magn. Mater.* **31-34**, 1257 (1983).
 [11] T. Idogaki, M. Hitaka, and K. Masuda, *J. Magn. Magn. Mater.* **140-144**, 1517 (1995).
 [12] H. Ueda, A. Tanaka, T. Iwashita, and T. Idogaki, *Phys. B: Condens. Matter* **284-288**, 1201 (2000).
 [13] M. E. J. Newman and R. M. Ziff, *Phys. Rev. Lett.* **85**, 4104 (2000).
 [14] M. E. J. Newman and R. M. Ziff, *Phys. Rev. E* **64**, 016706 (2001).
 [15] W. S. Oliveira, J. P. de Lima, N. C. Costa, and R. R. dos Santos, *Phys. Rev. E* **104**, 064122 (2021).
 [16] J. Hoshen and R. Kopelman, *Phys. Rev. B* **14**, 3438 (1976).
 [17] H. Kesten, *Commun. Math. Phys.* **74**, 41 (1980).
 [18] Y. Y. Tarasevich and S. C. Van der Mark, *Int. J. Mod. Phys. C* **10**, 1193 (1999).
 [19] M. Yanuka and R. Engelman, *J. Phys. A* **23**, L339 (1990).
 [20] M. I. González, P. Centres, W. Lebrecht, A. Ramirez-Pastor, and F. Nieto, *Physica A* **392**, 6330 (2013).
 [21] M. I. González-Flores, A. A. Torres, W. Lebrecht, and A. J. Ramirez-Pastor, *Phys. Rev. E* **104**, 014130 (2021).
 [22] A. Torres, M. González-Flores, W. Lebrecht, and A. Ramirez-Pastor, *Physica A* **604**, 127897 (2022).
 [23] F. Peruggi, F. di Liberto, and G. Monroy, *Physica A* **123**, 175 (1984).
 [24] Y. Y. Tarasevich and E. N. Manzhosova, *Int. J. Mod. Phys. C* **14**, 1405 (2003).